



The Low Dimensional Co-Based Nanorods as a Novel Platform for Selective Hydrogenation of Cinnamaldehyde

Tao Yuan¹ · Derong Liu¹ · Jianshan Gu¹ · Yongde Xia² · Yue Pan¹ · Wei Xiong¹

Received: 27 January 2019 / Accepted: 11 April 2019
© Springer Science+Business Media, LLC, part of Springer Nature 2019

Abstract

Since hydrogenation of C=C bond in the cinnamaldehyde is thermodynamically favored, the selective hydrogenation of C=O group is challenging. Developing effective catalysts for this transformation has been hindered by the intrinsic disadvantages of traditional materials for decades. Hereby, we report the synthesis of the low dimensional Co based nanorods (NRs) as the effective platform for C=O groups hydrogenation in the conjugated compounds. The Pt/Co-NRs catalyst is simply fabricated by loading the Pt nano-particles (NPs) on the Co-NRs and the stability of the Co-NRs support is improved by coordination between the Pt NPs and the pyridinic N ring. Resorting to XRD, FT-IR, XPS, HRTEM, DTG-TG characterization methods, the catalytic mechanism for C=O bond hydrogenation has been proposed. The synergistic effects of K⁺ and OH⁻ enhance the polarization of C=O group, leading to more adsorption of C=O groups on the Co-NRs so as to promote its hydrogenation performance. In the absence of spatial micropores in low dimensional Co based nanorods, the Pt/Co-NRs catalyst is more advantageous for mass transfer. Under optimal conditions, the conversion of cinnamaldehyde is 97.9% with 92.7% selectivity of cinnamyl alcohol within 3 h. In addition, the selectivity of cinnamyl alcohol changes slightly (only 2.4% fluctuations) after five recycle tests.

Keywords Low dimensional · Co based nanorods · Cinnamaldehyde · Selective hydrogenation · Cinnamyl alcohol

1 Introduction

Although cinnamyl alcohol is the important raw materials to produce flavouring, perfume and medicine [1, 2], the transformation of the selective hydrogenation of cinnamaldehyde is challenging. The preparation process of the catalyst for this transformation is also complex and tedious, which often involves high temperature or uncommon methods [3–6]. Besides MgO [7], high-valence metal oxides [8–10], GO [11] could be directly used as loading nano-scale metal particles materials without postmodifications and achieve a high selectivity to cinnamyl alcohol. In absence of activated sites that interact with and activate the C=O bond, most of traditional carriers including carbon materials [12], molecular

sieves [13] and polymers [14] could not compensate the thermodynamical difference in hydrogenation between C=O bond and C=C bond (in favour of the C=C group hydrogenation) in the conjugated compounds, which leads to the low catalytic efficiency for single C=O hydrogenation. Therefore, the way of modification traditional support by adding activated sites has been developed to deal with low catalytic efficiency for single C=O bond hydrogenation [15, 16].

Three dimensional Metal Organic Framework structure (MOFs) with intrinsic unsaturated metal sites has drawn much attention by virtue of the ordered and tuneable pores, large surface area, diverse structure which offer great potential to versatile applications especially in selective hydrogenation field [17, 18]. Those unsaturated metal sites in MOFs can be acted as Lewis acid sites that activate and lower the C=O bond energy of hydrogenation. Up to now, MOFs containing metal NPs have been intensively investigated on account of versatile and synergistic functionalities. Chen et al. [19] found that noble metal nanoparticles embedded in MOFs demonstrated novel properties due to the confinement effect and the structural flexibility of MOFs. The effect of the MOFs aperture size

✉ Wei Xiong
18875024416@163.com

¹ Institute of Chemistry and Chemical Engineering,
Chongqing University of Science and Technology,
Chongqing 401331, China

² College of Engineering, Mathematics and Physical Sciences,
University of Exeter, Exeter EX4 4QF, UK

and flexible structure on the final reaction yield distribution of selective hydrogenation to cinnamaldehyde was investigated by comparing Pt@ZIF-71 with Pt@ZIF-8 catalysts. Moreover, to induce better selectivity control on the encapsulated metal NPs@MOFs in catalytic selective hydrogenation reaction, Guo et al. [20] invented UIO-66-NH₂ confined Pt nanoclusters catalysts. The benefit of confining Pt NPs inside UIO-66-NH₂ is the high selectivity of 91.7% in contrast to less than 72% of the deposition of Pt NPs on the external surface of the UIO-66-NH₂. Besides, the confined Pt@UIO-66-NH₂ catalytic performance remains highly stable after repeated experiments. The only issue lies in the blockage of some micropores for the confined Pt@UIO-66-NH₂, thereby resulting in poor mass transport. To overcome this problem, Zhao et al. [21] developed the MOFs@NPs@MOFs catalyst, utilizing the epitaxial growth shell MIL-101 (Fe, Cr) layer as the selectivity regulator for the hydrogenation reactions. Exact regulation of the shell MIL-101 precursor concentration can achieve effective mass transport between the reactants and the products. In addition, those coordination unsaturated metal sites (CUSs) inside MIL-101 can act as Lewis acid sites that readily interact with the C=O bond and lower the reaction-barrier energy, which contributes to the C=O selective hydrogenation. Considering that the hydrophilic shell MIL-101 (Fe) is difficult to gather hydrophobic substrate, Yuan et al. [22] have applied conjugated micro- and mesoporous polymers with Iron(III) porphyrin (FeP-CMPs) to replace the shell MIL-101(Fe) and have innovated hydrophobic MIL-101@Pt@FeP-CMP. The porous and hydrophobic shell is superior to the hydrophilic MIL-101 (Fe) in gathering the hydrophobic reactants. Furthermore, Fe(III) ions in the FeP-CMPs is similar to the CUSs in MIL-101 that interacts with C=O bond and beneficially breaks the conjugated C=O bond. More interestingly, MIL-101@Pt@FeP-CMP can reach ultrahigh turnover frequency (TOF) of 1516.1 h⁻¹ with 97.3% selectivity towards cinnamyl alcohol and conversion of 97.6%.

Although the encapsulation of active metal nanoparticles on selected MOFs (Metal@MOFs) is an excellent way to promote the selectivity of unsaturated alcohol, the instability of the three dimensional MOFs structure, the complexity of catalyst-making and the high mass transfer resistance are important issues to be solved. To tackle these problems, low dimensional MOFs (nanosheet, nanorods, nanofiber) have been fabricated in the presence of PVP. Without space stereoscopic structure, the superiority of low dimensional MOFs in structure stability and mass transfer without loss of metal particles have been gaining extensive attention in catalysis [23–26]. To our knowledge, there has been no study in the open literature exploring the selective hydrogenation of the conjugated

C=C and C=O bond over low dimensional MOFs materials such as Co based nanorods.

Herein, the cinnamaldehyde selective hydrogenation is chosen as the model reaction, which is shown in Scheme 1. The low dimensional Co based nanorods with Pt NPs loading have been fabricated by a simple wet impregnation method. In contrast to Metal@MOFs type catalysts, the reaction transformation efficiency could be improved over the low dimensional Pt/Co-NRs catalyst. Moreover, the Pt/Co-NRs catalyst can achieve effective hydrogenation of single C=O bond without the aid of stereoscopic micropores.

2 Experimental

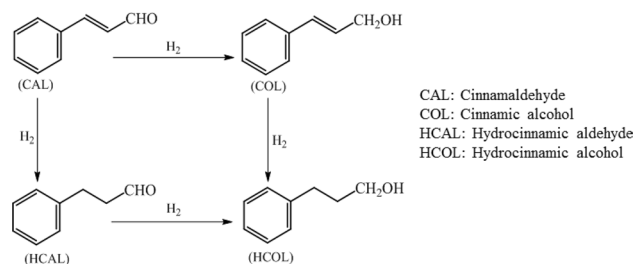
2.1 Chemicals

Cinnamaldehyde (AR, 95%) were used without purification, Chloroplatinic acid hexahydrate (H₂PtCl₆·6H₂O, AR, Pt 37.5%), Cobalt nitrate hexahydrate (Co(NO₃)₂·6H₂O, AR, 99%), 4,4-Bipyridine (AR, 98%), PVP (K-30) were purchased from Mackin, Potassium hydroxide (KOH, AR, 90%), Ethanol (AR, 99%) were purchased from ChengDu Chron Chemicals.

2.2 Synthesis of Pt/Co-NRs Catalyst

2.2.1 Synthesis of Pt Nanoparticles (NPs)

Pt NPs were synthesized according to the literature [27]. In a typical procedure, 50 mg PVP (K-30) was dissolved in 72 mL ethanol, and then 8.0 mL H₂PtCl₆ aqueous solution (10 mM) was added drop by drop. After stirring for 10 min at room temperature, the solution was refluxed in 150 mL flask for 3 h in air to obtain the PVP-stabilized Pt NPs. The concentration of the as-synthesized Pt NPs was about 1 mM, which were used without further treatment.



Scheme 1 Reaction pathways for selective hydrogenation of CAL

2.2.2 Synthesis of Co-NRs

Co based nanorods were synthesized according to the literature with minor modifications [28]. In a typical procedure, 400 mg PVP and 2 mmol 4,4-bipyridine were dissolved in 15 mL Ethanol, and another 15 mL ethanol containing 1 mmol $\text{Co}(\text{NO}_3)_2 \cdot 6\text{H}_2\text{O}$ was added into the above solution. The obtained aqueous mixture was stirred for 10 min. Subsequently, the solution was placed in a microwave vessel and sealed. The vessel was then rapidly heated to 100 °C, and was held at this temperature for 24 h. After cooling to room temperature, the solid products were collected by centrifugation at 12,000 rpm for 2 min and washed twice with ethanol. Finally, the obtained Co-NRs were placed in a vacuum drying oven at 80 °C overnight.

2.2.3 Preparation of Pt/Co-NRs Catalyst

A quota as-synthesized Pt NPs solution (1 mM) was added drop by drop into 20 mL ethanol containing 100 mg Co-NRs under vigorous stirring. Then the mixed solution was further stirred at room temperature for 2 h. Subsequently, the Pt/Co-NRs was collected by centrifugation at 12,000 rpm for 2 min and washed twice with ethanol. Finally, the obtained Pt/Co-NRs solid was redispersed in 10 mL ethanol, which was used as the catalyst for the cinnamaldehyde liquid-phase selective hydrogenation.

2.3 Catalyst Characterization

The Powder X-Ray diffraction (PXRD) scans of the synthesized Pt/Co-NRs catalysts were carried out from 5°–50° with an XRD-7000 X-ray diffractometer (CuK α radiation at 40 kV and 30 mA, Japan). The spectra of functional groups of the Pt/Co-NRs catalyst were confirmed using a Fourier transform infrared spectrum (FT-IR, KBr, 2000–500 cm^{-1}) BRUKE TENS OR27 (Germany). The elemental valence state and content of Pt and Co nanoparticles of the Pt/Co-NRs catalyst were measured by X-ray photoelectron spectroscopy (XPS, Kratos Axis Ultra DLD, UK) by a double anode Mg K α X-ray source (75 W) and an analyzer pass energy of 20 eV. The morphology and microstructure of the sample, the HAADF-STEM imaging and EDX mapping of Pt/Co-NRs catalysts were recorded by a high resolution electron microscopy (200 kV, FEI Talos F200x, America) and the samples were supported by carbon coated copper grids. The DTA-TG data of Pt/Co-NRs catalyst (10°C/min, 20–800°C, Ar) were recorded by STA 449 F3 instrument (Netzsch, Germany).

2.4 Selective Hydrogenation Reaction

The hydrogenation reaction was performed in a 0.1 L stainless steel autoclave equipped with a magnetic stirrer. 0.8 mmol cinnamaldehyde, 1 mL catalyst dosage (100 mg Pt/Co-NRs in 10 mL ethanol), 0.1 mL KOH (0.02 M) and 5 mL ethanol were added into the stainless autoclave in turn. The autoclave was kept sealed under hydrogen by purging with H_2 for 5 times. Then the autoclave was heated to 30 °C to start the reaction. After a period of reaction time, the autoclave was decompressed and the final liquid was analysed by an Agilent GC-6890N gas chromatography equipped with a FID detector and an Rtx-1 capillary column (30 m \times 0.25 mm \times 0.25 μm) with N_2 as the carrier gas.

3 Results and Discussion

3.1 Catalyst Analysis

To gain a better comprehensive understanding of the correlation between Pt/Co-NRs catalytic activity and structural features, the Pt/Co-NRs catalyst has been fully characterized by XRD, SEM, XPS, HRTEM, DTG-TG. The XRD patterns of Pt/Co-NRs catalyst with different Pt loadings are shown in Fig. 1. The peaks appearing at around 9.3°, 10.0°, 14.8°, 17.2°, 17.5°, 18.8°, 20.4°, 23.7° and 24.0° are originated from the Co-NRs. After 3% Pt NPs was loaded on the surface of Co-NRs, those peaks at $2\theta = 10.0^\circ$, 17.2°, 18.8°, 20.4° and 23.7° disappear, and the characteristic peaks for Co-NRs ($2\theta = 9.3^\circ$, 17.5°) turn weak, which completely disappear at 5% Pt NPs loading. The intensity of peak locating

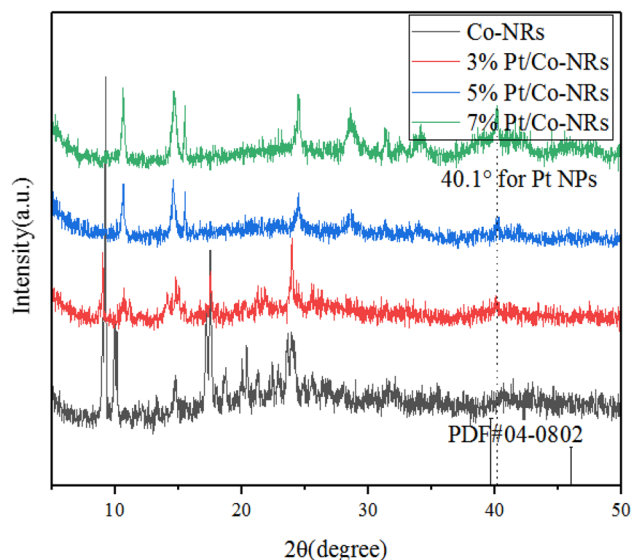


Fig. 1 The XRD patterns of the Pt/Co-NRs catalyst with various Pt loadings

at 14.8° increases as the Pt loading adds. Interestingly, the peak appears in 24° that is offset by 0.5° when Pt loading exceeds 5%. Moreover, with the addition of Pt, the occurrence of new peaks at $2\theta = 10.7^\circ$, 15.5° , 31.3° and 34.2° indicates the possible formation of new crystalline phase (Pt–N) between the Pt NPs and the Co-NRs carrier [29, 30]. Furthermore, the Peak appears at $2\theta = 40.1^\circ$ is from the Pt NPs (PDF No. 04-0802) and the Pt peak position is right offset by 0.3° , which also demonstrates the Pt NPs coordination with N atom in pyridine ring. The strong diffraction peak of Pt NPs reveals that the Pt NPs were successfully loaded on the surface of Co-NRs which is in accordance with the HRTEM result.

To further validate the interaction between Pt and the pyridinic N ring in Co-NRs, the FT-IR has been applied to confirm the coordination between the Pt NPs and the free pyridinic N atoms in Co-NRs. In Fig. 2, these peaks occurring at 1605 cm^{-1} are attributed to the C–N stretching vibrations of pyridine ring [31]. The strong peak at 1384 cm^{-1} is assigned to the NO_3^- antisymmetric stretching vibration of pyridine ring [32, 33]. After Pt NPs loading, the peak intensity attenuation of the C–N stretching vibration indicates the coordination of Pt NPs on the Co-NRs and the free N atoms from pyridine ring. Interestingly, the intensity of antisymmetric stretching vibration peak of NO_3^- (appearing at 1384 cm^{-1}) significantly decreases and then splits into another separate peaks at 1411 cm^{-1} , probably because the surface NO_3^- groups were concealed by the Pt NPs loading and herein reduces the intensity of NO_3^- antisymmetric stretching vibration in Co-NRs.

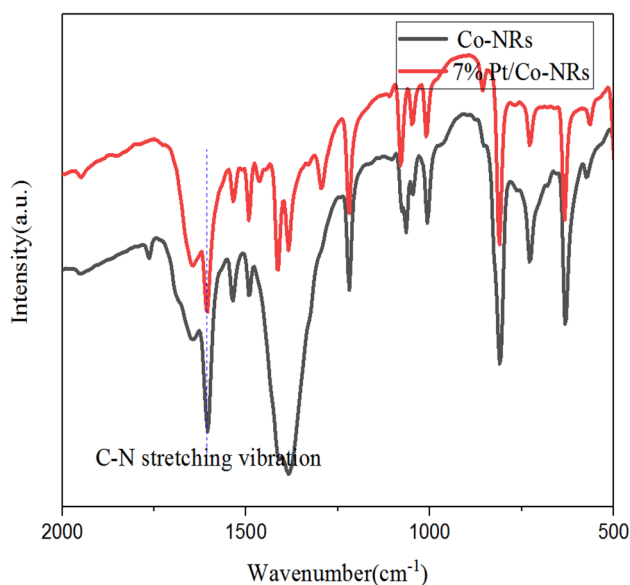


Fig. 2 The FT-IR spectra of the Co-NRs support and Pt/Co-NRs catalyst

Furthermore, to study the electron transfer between the Pt NPs and the Co-NRs, the XPS has been applied. In Fig. 3c, The N 1s peaks of Co-NRs occur at 399.7 and 406.8 eV. The 406.4 eV represents the N 1s shake-up peak, which is feature of the conjugated π system based pyridinic N [34]. But as Pt NPs are loaded, the disappearance of the unique shake-up peak (406.4 eV) reveals the transfer of the pyridinic N based conjugated π electron to Pt NPs [35]. Meanwhile, the binding energy of Pt $4f_{7/2}$ and Pt $4f_{5/2}$ (70.3 eV and 73.5 eV) is lower than that of metal Pt^0 (Pt^0 $4f_{7/2} = 70.9\text{--}71.3\text{ eV}$; Pt^0 $4f_{5/2} = 74.2\text{--}74.4\text{ eV}$ from XPS standard reference data in NIST), which implies that the Pt NPs obtains the electron from the conjugated π system in Pyridine ring. In addition, From the N 1s and Co 2p analysis, the binding energy of the Co–N coordinated system reduces by 0.8 eV compared with the original Co-NRs, which also suggests that part of the electrons transfer from the conjugated π system in pyridine ring to the Co–N coordinated system.

In order to elucidate the micro structure, components and active ingredient (Pt NPs) dispersion of the Pt/Co-NRs catalyst, the HRTEM with element mapping has been employed. The Co-NRs support shows rod-like structure with $88.1\text{ m}^2/\text{g}$ surface area in Fig. 4a. The nanorod structure remains unchanged and the surface area is $84.7\text{ m}^2/\text{g}$ after 7% Pt NPs are loaded on its surface. Moreover, the Pt NPs distribute homogeneously on the surface of Co-NRs and the size of Pt NPs closes to $1.8 \pm 0.5\text{ nm}$ (Fig. 4c). The lattice spacing of $d = 0.227\text{ nm}$ is from the Pt NPs. The element mapping images (Fig. 4f–i) clearly show the presence of the Pt, Co, N three elements in the Pt/Co-NRs catalyst and all of them are uniformly existed in the Pt/Co-NRs catalyst.

By comparing the DTG-TG profiles of Co-NRs and Pt/Co-NRs catalyst (Fig. 5), three weight losses are observable in Co-NRs TG profile at 250.2, 280.3 and 514.1°C , respectively. The weight loss at 250.2°C at a rate of $-5\%/ \text{min}$ is due to the Co-NRs degradation. The main weight loss of Co-NRs starts at 280.3°C at a rate of $-23.4\%/ \text{min}$, which declares that the Co-NRs matrix is completely degraded [36]. The third weight loss represents the carbonization of 4,4-bipyridine and PVP. The final materials contain Co, C, N elements at temperature higher than 514.1°C . However, the DTG-TG curve of Pt/Co-NRs shows weight loss at much lower rate. As shown in Fig. 5, the first weight loss occurs at 480.9°C at a rate of $-7.2\%/ \text{min}$ that its matrix starts to degrade and carbonization. Higher than 529.7°C , the ligands are carbonized into N doped carbon, which results in the weight loss and the residual weight is 34.67%. These results suggest that the Co-NRs stability is significantly strengthened by the addition of the Pt NPs, as a consequence of collective interaction between the Pt NPs and free pyridinic N, and between Pt NPs and the conjugated π system in pyridinic N ring.

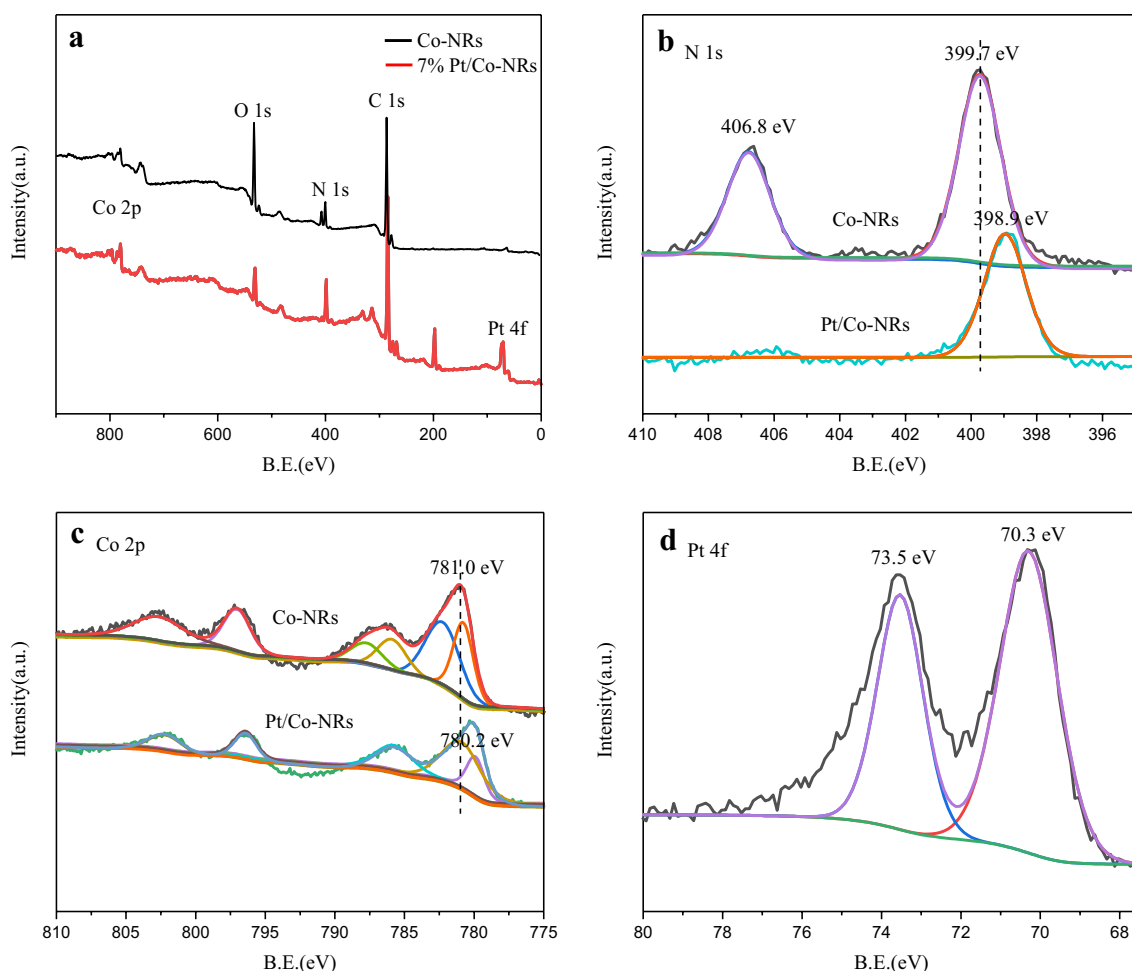


Fig. 3 The XPS profiles of the Co-NRs support and 7% Pt/Co-NRs catalyst (a); N 1s (b); Co 2p (c); Pt 4f (d)

3.2 Optimization of Reaction Conditions

After the micro structure features of the Pt/Co-NRs catalyst was analyzed, the catalytic performance of the Pt/Co-NRs was further studied. The results are summarized in Table 1, from which it can be observed that the Pt NPs mainly turn CAL into HCOL without single C=O bond hydrogenation. Conversely, the Co-NRs can provide much higher COL selectivity (83.3%) (Entry 2, in Table 1). With increasing addition of Pt, the conversion of CAL gradually increases but the COL selectivity shows a slow downward trend from 91.5 to 87.3%. So the 7% Pt loading (ICP test result is 6.8%) is chosen for the subsequent studies.

Table 2 lists the effect of base type on the catalytic activity. By the addition of KOH, the COL selectivity significantly increases from 12.9 to 90.5%. However, there is no major difference in the CAL conversion and COL selectivity among those inorganic and organic bases (Entry 2, 3, 4, 6, in Table 2). To find out the role of K^+ and OH^- in the promotion of the C=O bond hydrogenation, KCl solution

has employed to test the K^+ role in the polarization of C=O bond via the interaction between K^+ and the lone electron pair of oxygen atom in the C=O group. The COL selectivity increases from 12.9 to 47.9%, which is lower than OH^- in promotion the C=O bond hydrogenation. The OH^- mainly plays role in weakening the competitive adsorption of C=C bonds by the repulsion between π electron in C=C bond and OH^- anion in base solution, thus making the polarized C=O easily absorbed over Pt/Co-NRs catalyst [37].

Various reaction conditions including KOH concentration, H_2 pressure, reaction duration and solvent types were investigated for optimization of experimental conditions. The influence of KOH concentration on the 7% Pt/Co-NRs catalytic activity is presented in Fig. 6a. The CAL conversion declines from 97.9 to 56.1% with increasing KOH concentration because the base solution is unfavorable for the H_2 dissociation over the Pt NPs. Conversely, the COL selectivity increases from 12.9 to 91.6%. The HCOL and HCOL selectivity have a similarly downward trend. As the H_2 pressure goes up (Fig. 6b), the CAL conversion increases

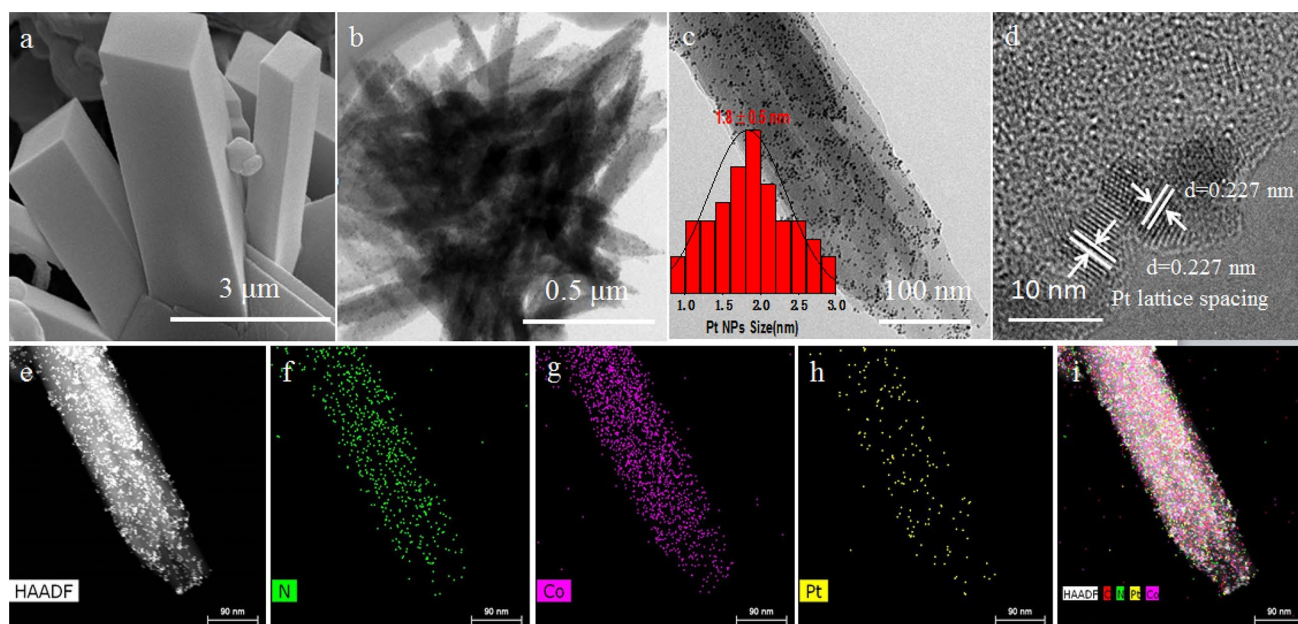


Fig. 4 The SEM images of Co-NRs (a), 7% Pt/Co-NRs (b–d) [the inserted figure in (c): the Pt NPs size distribution diagram]; the HAADF-STEM image (e), and element mapping of N (f), Co (g), Pt (h), all (i)

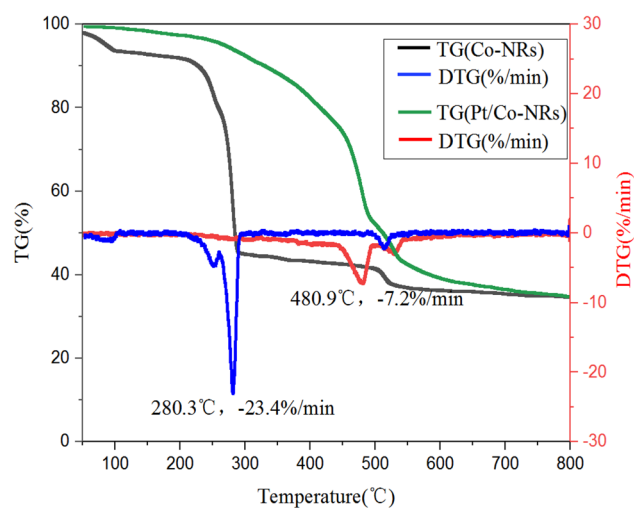


Fig. 5 The DTG-TG profiles of the Co-NRs support and 7% Pt/Co-NRs catalyst

from 52.5 to 90.2%. Surprisingly, the COL selectivity does not change significantly and hold at 88.5–90.5%. However the HCAL and HCOL selectivity have an opposite trend that H_2 pressure increase results in further hydrogenation transformation of the HCAL and COL to HCOL, so that the HCOL selectivity increases from 4.4 to 10.9%. Furthermore, the reaction duration mainly affects the CAL conversion (Fig. 6c). With the time extending to 180 min, the CAL conversion increases from 60.5 to 97.9%, while the COL selectivity changes slightly (only 5.8 fluctuations). In addition,

Table 1 The influence of Pt loading on catalytic performance

Entry	Catalyst	Conversion	Selectivity		
			COL	HCAL	HCOL
1	Pt NPs	100	0.1	24.3	51.6
2	Co-NRs	13.0	83.3	4.8	11.9
3	3%Pt/Co-NRs	19.9	91.5	8.4	0
4	5%Pt/Co-NRs	56.3	90.9	5.6	3.4
5	7%Pt/Co-NRs	80.5	90.5	4.1	5.4
6	9%Pt/Co-NRs	85.6	87.3	5.3	7.3

Reaction conditions: 0.45 mg Pt (Entry 1); 1 mL catalyst dosage (100 mg catalyst dispersion into 10 mL ethanol) (from Entry 2 to Entry 6), 0.8 mmol cinnamaldehyde, 30 °C, 2 MPa H_2 , 0.1 mL KOH (0.02 M), 5 mL ethanol, 120 min

Table 2 The comparison of different base type for influence catalytic activity

Entry	Base type	Conversion	Selectivity		
			COL	HCAL	HCOL
1	No	97.9	12.9	6.4	79.6
2	NaOH	76.7	89.5	4.6	5.8
3	KOH	80.5	90.5	4.1	5.4
4	K_2CO_3	77.9	89.1	4.8	6.1
5	KCl	96.2	47.9	20.8	31.3
6	Ethylenediamine	78.9	86.0	6.5	7.5

Reaction conditions: 1 mL catalyst dosage (100 mg 7% Pt/Co-NRs catalyst dispersion into 10 mL ethanol and each 1 mL ethanol containing 0.68 mg Pt NPs), 0.8 mmol cinnamaldehyde, 30 °C, 2 MPa H_2 , base concentration (0.02 M), 5 mL ethanol, 120 min

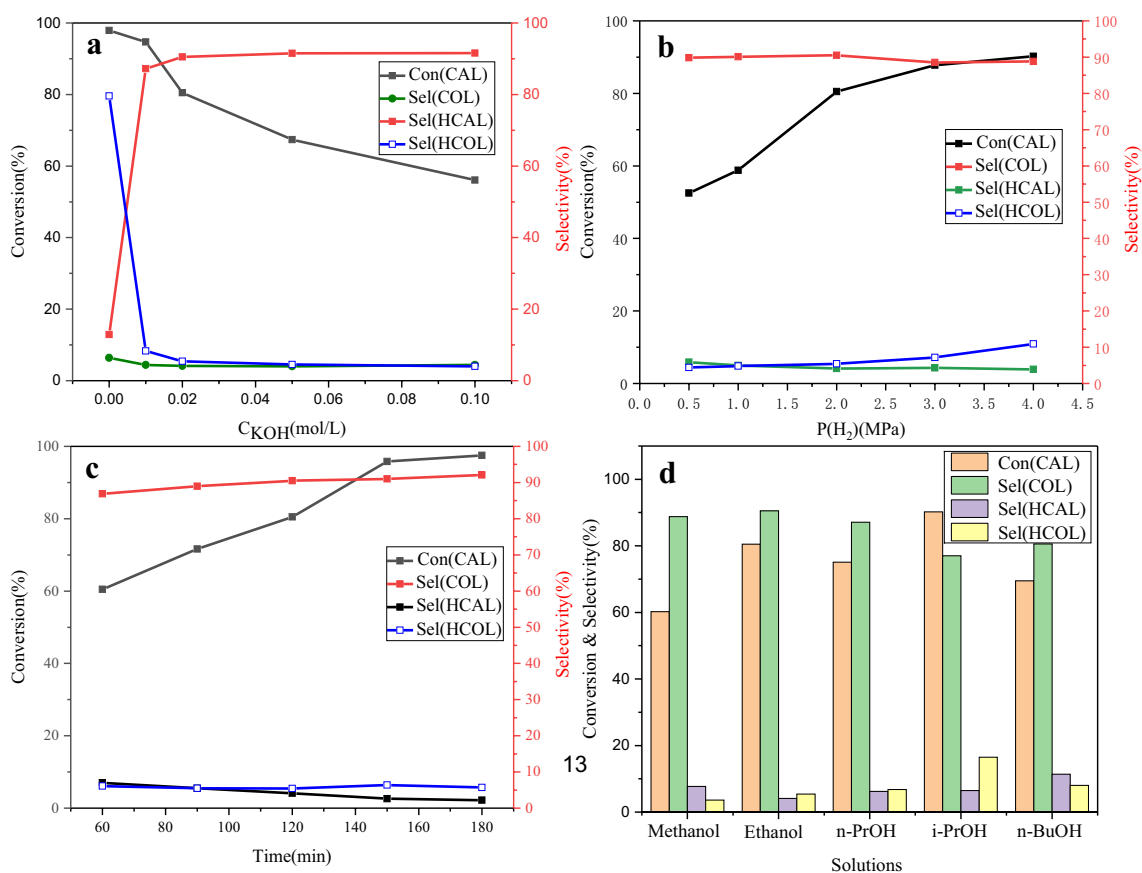


Fig. 6 **a** Reaction condition: 1 mL catalyst dosage (100 mg 7% Pt/Co-NRs catalyst dispersion into 10 mL ethanol and each 1 mL ethanol containing 0.68 mg Pt NPs), 0.8 mmol cinnamadehyde, 30 °C, 2 MPa (H_2), 0.1 mL KOH (different concentration), 5 mL ethanol, 180 min; **b** reaction condition: 1 mL Catalyst dosage (100 mg 7% Pt/Co-NRs catalyst dispersion into 10 mL ethanol and each 1 mL ethanol containing 0.68 mg Pt NPs), 0.8 mmol cinnamaldehyde, 30 °C, 0.1 KOH (0.02 M), 5 mL ethanol, 180 min; **c** reaction condition: 1 mL catalyst

dosage (100 mg 7% Pt/Co-NRs catalyst dispersion into 10 mL ethanol and each 1 mL ethanol containing 0.68 mg Pt NPs), 0.8 mmol cinnamadehyde, 30 °C, 2 MPa H_2 , 0.1 KOH (0.02 M), 5 mL ethanol; **d** reaction condition: 1 mL catalyst dosage (100 mg 7% Pt/Co-NRs catalyst dispersion into 10 mL ethanol and each 1 mL ethanol containing 0.68 mg Pt NPs), 0.8 mmol cinnamaldehyde, 30 °C, 2 MPa H_2 , 0.1 KOH (0.02 M), 180 min

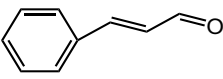
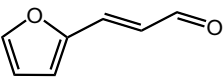
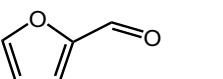
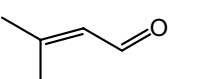
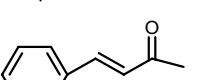
the time prolonging is beneficial to the HCOL conversion at a sacrifice of the HCAL selectivity. Finally, we studied the influence of polar solvents on the Pt/Co-NRs catalytic activity (Fig. 6d). The polar solvents including methanol, ethanol and i-PrOH are beneficial to both the conversion and selectivity. It has been confirmed that C=O group polarization could be enhanced via the hydrogen bond formation in low-molecular weight alcohols, thereby increase the COL selectivity [38, 39]. Among these solvents, the ethanol gives 80.5% CAL conversion and 90.5% COL selectivity. Table 3 lists the Pt/Co-NRs catalytic activity for various α , β -unsaturated aldehyde (ketone). From Table 3, it is clear that α , β -unsaturated aldehyde with different substituents and the position of substituent greatly affect the reaction conversion and selectivity. The cinnamaldehyde conversion is up to 97.9%, but the 3-(2-furyl) acrolein and furfural conversion only gains 59.0% and 69.9%, respectively, which indicates that the presence of electron donating substitute (the electron

cloud density of furan group is higher than that of benzene) is adverse for the reaction conversion. The electron donating substitute leads to the electron cloud density increase in the conjugated C=C and C=O system that is hard for reduction. Steric hindrance is an important factor to affect the selectivity of C=O group hydrogenation. By contrast to Entries 1 and 4, there exists larger spatial steric hindrance close to the C=C bond end, which is beneficial for the C=O group hydrogenation.

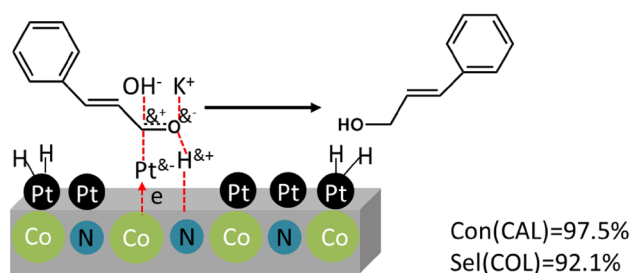
As a consequence, the position of the electron-donating substitute next to the C=O bond end is extremely hostile for the benzalacetone hydrogenation and results in low conversion (45.8%) and selectivity (12.1%).

In Fig. 7, the catalytic mechanism has been proposed to explain the efficient hydrogenation of C=O group over the Pt/Co-NRs catalyst. Based on above experimental data, the Co-NRs mainly determine the selectivity of C=O hydrogenation. And the Pt NPs take charge of H_2 dissociation

Table 3 Selective hydrogenation of different α , β -unsaturated aldehyde (ketone) with 7% Pt/Co-NRs catalyst

Entry	Substrates	Conversion	Selectivity		
			C=O	C=C	All
1		97.9	92.7	1.8	5.6
2		59.0	92.8	3.5	5.6
3		69.9	100	0	0
4		64.5	69.1	25.2	5.7
5		48.5	12.1	78.4	6.7

Reaction conditions: 1 mL catalyst dosage (100 mg 7% Pt/Co-NRs catalyst dispersion into 10 mL ethanol and each 1 mL ethanol containing 0.68 mg Pt NPs), 0.8 mmol substrates, 30 °C, 2 MPa (H_2), 0.1 mL KOH (0.02 M), 5 mL ethanol, 180 min

**Fig. 7** The proposed catalytic mechanism for the 7% Pt/Co-NRs catalyst

and control the conversion of cinnamaldehyde transformation. The XPS results show that the Co-NRs with partial negative charge is favored for the polarized C=O group adsorption. Meanwhile, the π -electron in the C=C bond is easily rejected by the surface OH^- anion and the $Pt^{\delta-}$ with enhanced electronic density that favor a d-electron feedback into the π^* orbit of the polar C=O group [40, 41] and leads to less hydrogenation of the C=C group on the surface of Pt/Co-NRs catalyst. Besides, the synergistic effects of K^+ and OH^- enhance the C=O bond polarization and thereby increase the C=O group hydrogenation.

Among the reported catalysts, selecting microporous and mesoporous materials with the shape-selective effect such as MOFs, meso- SiO_2 , SBA as the catalyst carrier (like metals encapsulation) is an excellent method to solve the low selectivity of C=O hydrogenation in the cinnamaldehyde. These materials can not only effectively control the size of noble metal in the pore, but also regulate the way of substrate adsorption that allows the low steric hindrance to pass into the pore and reacts with the active ingredients. However, the metals encapsulation structure is bad for the mass transfer and prolongs the reaction time. Besides, the complexity of catalyst-making and instability of the material structure are urgent issues to cope with. Therefore, the low dimensional Co based nanorods reported in this study could provide a novel platform for the selective hydrogenation of cinnamaldehyde, which is compared with other reported catalysts for the CAL hydrogenation and presented in Table 4.

Figure 8 shows that the 7% Pt/Co-NRs catalyst maintains the COL selectivity of 90.3–92.7% (only 2.4% fluctuations) and CAL conversion of 77.8% after five recycle tests. The HRTEM has been applied to study the reason for the loss of catalytic activity of Pt/Co-NRs catalyst.

The HRTEM image in Fig. 9 shows that the Co-based nanorods keep integrity and there is not any Pt NPs agglomeration. The Pt NPs particle size is around 2.17 ± 0.38 nm that is slightly larger than the initial Pt NPs size (1.8 ± 0.5 nm). It is likely that the migration of Pt NPs accounts for the Pt NPs slight aggregation during the

Table 4 Comparison of the activity of reported catalysts for the CAL hydrogenation to COL

Catalysts	Pt content (wt%)	Reaction time (h)	Conv. (CAL) (%)	Sel. (COL) (%)	Ref.
Pt@ZIF-8	1	6	58.6	88.7	[19]
Pt@ZIF-71	1	6	11.2	96.9	[19]
Pt@UIO-66-NH ₂	10.7	42	85.9	87.9	[20]
Pt/mSiO ₂	1	10	52	93	[42]
MIL-101(Cr)@Pt@MIL-101(Fe)	5	20	90.6	94.3	[21]
Pt/mTiO ₂ -SiO ₂	2	5	99.0	63.8	[43]
Co-Pt/SBA-15	3	2	71	91	[44]
Pt/Co-NRs	6.8	3	97.5	92.1	This work

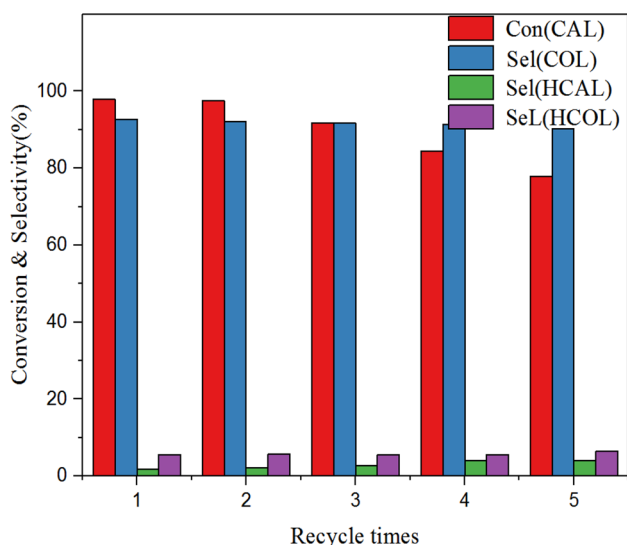


Fig. 8 The recycle test of the 7%Pt/Co-NRs catalyst for CAL hydrogenation

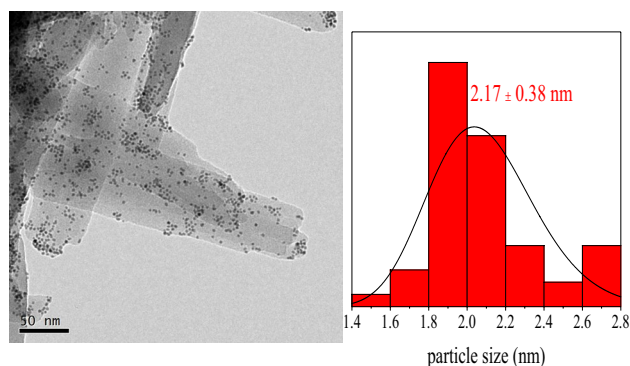


Fig. 9 HRTEM image of the used Pt/Co-NRs catalyst and the Pt NPs size distribution histogram

liquid-phase catalytic tests, which may bring about the loss of the catalytic activity of Pt/Co-NRs materials.

4 Conclusions

The one-dimensional Co-NRs nanorods with Pt NPs loading have been synthesized by a simple wet impregnation method. The obtained Pt/Co-NRs catalyst has an excellent catalytic activity for cinnamaldehyde transformation to cinnamyl alcohol with the subtle aid of KOH. In addition, the addition of the Pt NPs changes the stability of the Co-NRs carrier and keeps the Co-NRs structural integrity up to 514.1 °C. Moreover, without spatial micropores in one-dimensional Pt/Co-NRs, it is more beneficial for mass transfer between Pt NPs and cinnamaldehyde. Under the optimal

condition, the Pt/Co-NRs catalyst can achieve 97.5% CAL conversion with 92.7% COL selectivity within 3 h. After five recycle tests, the Pt/Co-NRs catalyst can still maintain the high COL selectivity (only 2.4% fluctuations).

Acknowledgements The authors are grateful for the financial support from the Basic and Frontier Research Project of Chongqing in China (No. cstc2016jcyjA0139). I gratefully acknowledge myself and Pro Xia for having revised this manuscript on New year's Day in 2019.

Compliance with Ethical Standards

Conflict of interest The authors declare that they have no conflict of interest.

References

- Mäki-Arvela P, Hájek J, Salmi T, Murzin DY (2005) *Appl Catal A* 292:1–49
- Blaser H-U, Malan C, Pugin B, Spindler F, Steiner H, Studer M (2003) *Adv Synth Catal* 345:103–151
- Liu X, Cheng S, Long J, Zhang W, Liu X, Wei D (2017) *Mater Chem Front* 1:2005–2012
- Hu Q, Wang S, Gao Z, Li Y, Zhang Q, Xiang Q et al (2017) *Appl Catal B* 218:591–599
- Song S, Liu X, Li J, Pan J, Wang F, Xing Y et al (2017) *Adv Mater* 29:1700495
- Hao C-H, Guo X-N, Pan Y-T, Chen S, Jiao Z-F, Yang H et al (2016) *J Am Chem Soc* 138:9361–9364
- Siddiqui N, Sarkar B, Pendem C, Khatun R, Sivakumar Konthala LN, Sasaki T et al (2017) *Catal Sci Technol* 7:2828–2837
- Piqueras CM, Puccia V, Vega DA, Volpe MA (2016) *Appl Catal B* 185:265–271
- He S, Xie L, Che M, Chan HC, Yang L, Shi Z et al (2016) *J Mol Catal A* 425:248–254
- Wei S, Zhao Y, Fan G, Yang L, Li F (2017) *Chem Eng J* 322:234–245
- Ji X, Niu X, Li B, Han Q, Yuan F, Zaera F et al (2014) *Chem-CatChem* 6:3246–3253
- Chen S, Meng L, Chen B, Chen W, Duan X, Huang X et al (2017) *ACS Catal* 7:2074–2087
- Zhang Y, Chen C, Gong W-B, Song J-Y, Su Y-P, Zhang H-M et al (2017) *Chin J Chem Phys* 30:467–473
- Pan H, Li J, Lu J, Wang G, Xie W, Wu P et al (2017) *J Catal* 354:24–36
- Ramosfernandez E, Ferreira A, Sepulvedaescribano A, Kapteijn F, Rodriguezreinoso F (2008) *Enhancing. J Catal* 258:52–60
- Chen X, Zhu H, Song X, Du H, Wang T, Zhao Z et al (2017) *React Kinet Mech Cat* 120:637–649
- Hu S, Liu M, Ding F, Song C, Zhang G, Guo X (2016) *J CO2 Util* 15:89–95.
- Yuan Q, Zhang D, Haandel LV, Ye F, Xue T, Hensen EJM et al (2015) *J Mol Catal A* 406:58–64
- Chen L, Zhan W, Fang H, Cao Z, Yuan C, Xie Z et al (2017) *Chem Eur J* 23:11397–11403
- Guo Z, Xiao C, Maligalganesh RV, Zhou L, Tian WG, Li X et al (2014) *ACS Catal* 4:1340–1348
- Zhao M, Yuan K, Wang Y, Li G, Guo J, Gu L et al (2016) *Nature* 539:76–80
- Yuan K, Song T, Wang D, Zhang X, Gao X, Zou Y et al (2018) *Angew Chem Int Ed Engl* 57:5708–5713

23. Liu J, Yu H, Wang L, Deng Z, Naveed K-U-R, Nazir A et al (2018) *Inorg Chim Acta* 483:550–564
24. Zhu W, Zhang C, Li Q, Xiong L, Chen R, Wan X et al (2018) *Appl Catal B* 238:339–345
25. Liang Y, Shang R, Lu J, Liu L, Hu J, Cui W (2018) *ACS Appl Mater Inter* 10:8758–8769
26. Zhao L, Dong B, Li S, Zhou L, Lai L, Wang Z et al (2017) *ACS Nano* 11:5800–5807
27. Teranishi T, Hosoe M, Tanaka T, Miyake M (1999) *J Phys Chem B* 103:3818–3827
28. Lin Y, Wan H, Chen F, Liu X, Ma R, Sasaki T (2018) *Dalton Trans* 47:7694–7700
29. Ning X, Yu H, Peng F, Wang H (2015) *J Catal* 325:136–144
30. Bolzan GR, Abarca G, Gonçalves WDG, Matos CF, Santos MJL, Dupont J (2018) *Chem Eur J* 24:1365–1372
31. Lu J, Yu C, Niu T, Paliwala T, Crisci G, Somosa F et al (1998) *Inorg Chem* 37:4637–4640
32. Zhuang Z, Cheng J, Wang X, Zhao B, Han X, Luo Y (2007) *Spectrochim Acta A* 67:509–516
33. Topaçlı A, Akyüz S (1995) *Spectrochim Acta A* 51:633–641
34. Keane MP, de Brito AN, Correia N, Svensson S, Lunell S (1991) *Chem Phys* 155:379–387
35. Clark DT, Adams DB, Dilks A, Peeling J, Thomas HR (1976) *J Electron Spectrosc Relat Phenom* 8:51–60
36. Liao J-H, Cheng S-H, Su C-T (2002) *Inorg Chem Commun* 5:761–764
37. Leng F, Gerber IC, Axet MR, Serp P (2017) *Chim* 21:346–353
38. Singh UK, Vannice MA (2001) *Appl Catal A* 213:1–24
39. Manikandan D, Divakar D, Sivakumar T (2007) *Catal Commun* 8:1781–1786
40. He S, Shao Z-J, Shu Y, Shi Z, Gao X-M, Gao Q, Hu P, Tang Y (2016) *Chem Eur J* 22:5698–5704
41. Chen T, Shi Z, Zhang G, Chan H-C, Shu Y, Gao Q, Tang Y (2018) *ACS Appl Mater Interface* 10:42475–42483
42. Prashar AK, Mayadevi S, Nandini Devi R (2012) *Catal Commun* 28:42–46
43. Wu Q, Zhang C, Zhang B, Li X, Ying Z, Liu T et al (2016) *J Colloid Interface Sci* 463:75–82
44. Zheng Q, Wang D, Yuan F, Han Q, Dong Y, Liu Y et al (2016) *Catal Lett* 146:1535–1543